Detection and Discrimination of Open-Phase Fault in Permanent Magnet Synchronous Motor Drive System

Jun Hang, *Student Member, IEEE*, Jianzhong Zhang, *Member, IEEE*, Ming Cheng, *Fellow, IEEE*, and Shichuan Ding, *Member, IEEE*

***Abstract*—Open-phase fault in permanent magnet synchronous motor (PMSM) drive system occurs as the phase winding is disconnected or one leg of the inverter bridge fails. It may generate large electromagnetic torque ripple and serious mechanical vibration. Therefore, a rapid fault detection method is greatly required to identify this fault at early stage and prevent damage to the system. This paper develops a method of the open-phase fault detection and discrimination for the PMSM drive system based on the zero-sequence voltage components, in which the discrimination of the fault types, namely internal stator winding failure and switches failure of the inverter is realized. Then, appropriate fault-tolerant measures may be taken according to the different fault types. The experimental platform is established, and the experimental results verify the effectiveness of the proposed method, showing that not only the open-phase fault can be rapidly detected, but also the fault type can be effectively discriminated.**

***Index Terms*—Fault diagnosis, frequency tracking, open-phase fault, permanent magnet machine, zero-sequence voltage components (ZSVC).**

I. Introduction

DUE to its high power density, high efficiency, and high torque density, permanent magnet synchronous motor (PMSM) is widely used in modern wind energy conversion system [1] and transportation, such as electrical vehicles and subway [2], [3], where the high reliability is of great importance. An undetected fault in the PMSM drive system may lead to very high repair or replacement cost, or even catastrophic failure. Therefore, fault detection is greatly needed, which may realize the scheduling preventive maintenance for the drive system [4].

Open-phase fault usually appears as the phase winding of the PMSM is disconnected with the power source, which may be caused by internal stator winding failure (ISWF), two switches failure (TSF) of the same leg in the inverter. or mechanical failure of the machine terminal connector [5]. The widely used three-phase PMSM drive system is shown in Fig. 1 and the open-phase fault is the common fault for such drive system. The open-phase fault causes large electromagnetic torque ripples and serious mechanical vibration. If this fault is not detected in time and remedial measures are not taken, the successive operation of the PMSM may cause the secondary damage, even catastrophic failure to the overall system.

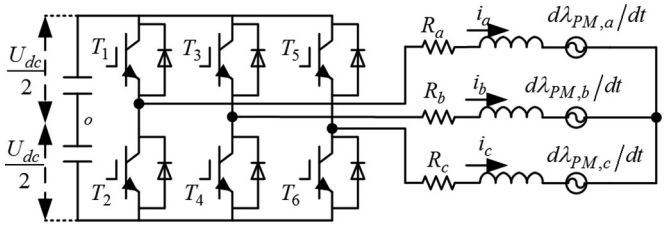

Fig. 1. Configuration of a three-phase PMSM drive system.

In recent years, a few detection methods have been put forward for the open-phase fault. In [6], the open-phase fault is judged by the root-mean-square (RMS) value of phase currents. In this method, the residual signature generated based on the RMS value is compared with the chosen threshold to detect the open-phase fault and identify the phase in which the fault occurs. In [7], the open-phase fault is detected by frequency domain analysis and $\alpha\beta$ current signature. Frequency-domain analysis method clearly detects the open-phase fault by monitoring the amplitude of the third harmonic of the phase current, and, then, $\alpha\beta$ current signature is used to identify the faulty phase. The methods proposed in [6] and [7] may detect the open-phase fault correctly. However, these methods require a relatively long detection time which exceeds one electrical cycle. Furthermore, extra memory space is required for storing phase currents, $\alpha\beta$ current, and their treatment results. Some rapid detection methods for the open-phase fault are proposed in literatures [8] and [9]. In [8], the predictive method for the single open-phase fault detection is presented, which is based on the difference between actual stator current and its predicted value. The magnitude of the difference serves as a main diagnostic index for the open-phase fault detection, and the fault location is identified by the angle of the stator current. In [9], an open-phase fault detection method is developed based on *DQ* current signature. In this method, a fault indicator defined by the currents i_{ds}^r and i_{qs}^r is used for the open-phase fault detection, and the phase difference between the actual electrical angle and the quantity $\tan^{-1}(-i_{qs}^r/i_{ds}^r)$ is applied to locate the faulty phase. The current-signals-based detection methods proposed in [6]–[9] can exactly detect the open-phase fault. However, the proposed methods cannot discriminate the fault types due to the same waveforms of the stator currents under different fault types, such as ISWF and TSF. In addition, there are a few fast fault detection methods based on voltage signals [10]–[15]. In [10], the detection and identification of the power

Manuscript received December 29, 2014; revised May 31, 2015 and August 20, 2015; accepted September 6, 2015. Date of publication September 16, 2015; date of current version January 28, 2016. This work was supported in part by the National Key Basic Research Program of China (973 Program) (2013CB035603) and the National Natural Science Foundation of China (51137001, 51320105002). Recommended for publication by Associate Editor K.-B. Lee.

The authors are with the School of Electrical Engineering, Southeast University, Nanjing 210096, China (e-mail: jun_hang511@163.com; jiz@seu.edu.cn; mcheng@seu.edu.cn; dingsc@126.com).

Color versions of one or more of the figures in this paper are available online at http://ieeexplore.ieee.org.

Digital Object Identifier 10.1109/TPEL.2015.2479399

switch is accomplished by evaluating the residual signals deriving from a direct comparison of the measured voltages to their respective references. In [11], a fast-diagnostic method for the open-switch fault is implemented by combining the collector–emitter voltage of lower switch for each inverter leg and the reference switching signals. In [12], the gate-voltage behavior at turn-on transient of the IGBTs is adapted to detect failures of short-circuit and open-circuit in the IGBT. In [13], a voltage measurement-based sectoral diagnosis method is presented for the open switch faults of PMSM drives, in which the sectoral average of the difference between the reference and the measured pole voltage is directly compared with the threshold to achieve the open fault detection of each switch. In [14], the open-circuit fault detection and identification is achieved by the voltage distortion observer. The voltage distortions are estimated by the model reference adaptive system technique, and, then, compared with the preset threshold value to determine the fault condition. In [15], a voltage-based approach is proposed for open-circuit fault diagnosis in closed-loop controlled PWM ac voltage source converters by the reference voltages available from the control system. These methods presented in [10]–[15] can quickly implement fault detection and location. However, these methods mainly focus on individual or multiple switch fault detection rather than the open-phase fault.

Since the open-phase fault may be caused by different parts, the appropriate fault--tolerant measures for the different fault types can be taken with the consideration of the feature, implementation costs, and performance limitations of each of the fault-tolerant methods [16]. For example, reconfiguration of the inverter may be adopted as the TSF occurs, where the performances of the PMSM at postfault operation are the same as those at prefault operation [17], [18]. For the ISWF, two-phase fault-tolerant operation for the PMSM drive system may be adopted, keeping the maximum output torque unvaried [19], [20]. Hence, it is of importance not only for the detection of the open-phase fault, but also for the discrimination of the fault types. However, to the authors' knowledge, the previous literatures mostly focus on the open-phase fault detection. The discrimination of the fault types is rarely studied so far. Hence, this paper aims to fill this gap, namely the discrimination of the fault types.

This paper first proposes a method of the open-phase fault detection and discrimination for the PMSM drive system, which is based on zero-sequence voltage components (ZSVC). The proposed method not only detects the open-phase fault rapidly but also discriminates the fault types, such as ISWF and TSF. By detecting, locating, and discriminating the fault, appropriate fault-tolerant measures might be applied to the PMSM drive system, and fault-tolerant measure is out of the scope of this paper and will be not discussed in this paper. In addition, only single open-phase fault is considered in this paper since the three-phase PMSM cannot work under the condition of two or more open-phase fault.

II. Proposed Method

The method based on the ZSVC has been used in the fault diagnosis and achieves good performance. In [21]–[23], the ZSVC-based interturn fault detection for the PMSM is studied. However, this paper differs from the previous studies in the fact that the ZSVC is used for the detection and discrimination of the open-phase fault, where the fault type only includes ISWF and TSF since the terminal connector failure has the same symptom as the ISWF and might be treated by same method.

A. Healthy Condition

The voltage equations of three-phase healthy PMSM in *abc* reference frame are expressed as

$$\begin{cases} V_a = R_s i_a + L\dfrac{di_a}{dt} + M\dfrac{di_b}{dt} + M\dfrac{di_c}{dt} + \dfrac{d\lambda_{\mathrm{PM},a}}{dt} + V_0 \\ V_b = R_s i_b + M\dfrac{di_a}{dt} + L\dfrac{di_b}{dt} + M\dfrac{di_c}{dt} + \dfrac{d\lambda_{\mathrm{PM},b}}{dt} + V_0 \\ V_c = R_s i_c + M\dfrac{di_a}{dt} + M\dfrac{di_b}{dt} + L\dfrac{di_c}{dt} + \dfrac{d\lambda_{\mathrm{PM},c}}{dt} + V_0 \end{cases} \tag{1}$$

where V_a, V_b, and V_c are the phase voltages, i_a, i_b, and i_c are the phase currents, R_s is the phase stator resistance, L is the phase stator self-inductance, M is the mutual-inductance between the stator phases, and V_0 is the voltage difference between the neutral point of the stator windings and the dc midpoint of the electronic inverter. $\lambda_{\mathrm{PM},a}$, $\lambda_{\mathrm{PM},b}$, and $\lambda_{\mathrm{PM},c}$ are the flux in the phases *a*, *b,* and *c* due to permanent magnets, respectively. They are expressed as [21]:

$$\begin{cases} \lambda_{\mathrm{PM},a} = \lambda_{\mathrm{PM},1}\cos(\theta) + \sum\limits_{v=2k+1} \lambda_{\mathrm{PM},v}\cos(v\theta - \theta_v) \\ \lambda_{\mathrm{PM},b} = \lambda_{\mathrm{PM},1}\cos\left(\theta - \dfrac{2\pi}{3}\right) \\ \qquad\qquad + \sum\limits_{v=2k+1} \lambda_{\mathrm{PM},v}\cos\left(v\theta - \theta_v - 2v\dfrac{\pi}{3}\right) \\ \lambda_{\mathrm{PM},c} = \lambda_{\mathrm{PM},1}\cos\left(\theta + \dfrac{2\pi}{3}\right) \\ \qquad\qquad + \sum\limits_{v=2k+1} \lambda_{\mathrm{PM},v}\cos\left(v\theta - \theta_v + 2v\dfrac{\pi}{3}\right) \end{cases} \tag{2}$$

where k is a positive integer, $\lambda_{\mathrm{PM},1}$ is the amplitude of the fundamental magnet flux, $\lambda_{\mathrm{PM},v}$ is the amplitude of the vth harmonic magnet flux, θ is the rotor electrical position, and θ_v is the angle between the vth harmonic magnet flux and the fundamental one.

In the wye-connected PMSM, the following condition is satisfied:

$$i_a + i_b + i_c = 0. \tag{3}$$

By adding three rows of (1) and considering (2) and (3), the expression of the ZSVC V_0 is obtained as

$$V_0 = \frac{1}{3}(V_a + V_b + V_c) - \frac{d\lambda_{\mathrm{PM},0}}{dt} \tag{4}$$

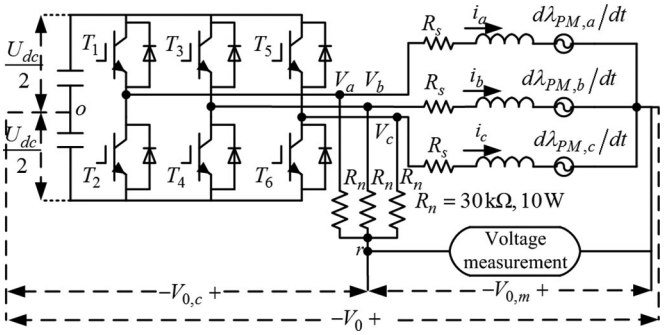

Fig. 2. PMSM showing the resistor network used to generate an artificial neutral point.

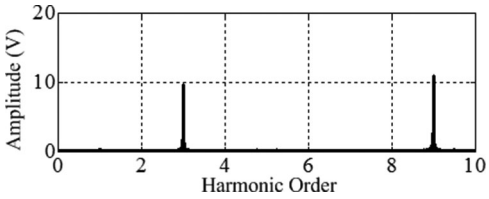

Fig. 3. FFT result of experimental ZSVC $V_{0,m}$ for the healthy PMSM, under 30% rated load at 720 r/min.

where

$$\lambda_{\mathrm{PM},0} = (\lambda_{\mathrm{PM},a} + \lambda_{\mathrm{PM},b} + \lambda_{\mathrm{PM},c})/3 = \sum_{v=3n,n=1,3,5\cdots} \lambda_{\mathrm{PM},v} \cos(v\theta - \theta_v). \quad (5)$$

In this paper, the resistor network is used to generate an artificial neutral point, as shown in Fig. 2. The sum of currents through the three branches of the balanced resistor network is equal to zero, and it has

$$\frac{V_a - V_{0,c}}{R_n} + \frac{V_b - V_{0,c}}{R_n} + \frac{V_c - V_{0,c}}{R_n} = 0. \quad (6)$$

From (6), it has

$$V_{0,c} = (V_a + V_b + V_c)/3 \quad (7)$$

where

$$V_0 = V_{0,c} + V_{0,m}. \quad (8)$$

By substituting (4) and (7) into (8), the ZSVC $V_{0,m}$ is expressed as

$$V_{0,m} = -\frac{d\lambda_{\mathrm{PM},0}}{dt}. \quad (9)$$

According to (9), it can be seen that the ZSVC $V_{0,m}$ only depends on the time derivative of the $\lambda_{\mathrm{PM},0}$ in a healthy PMSM. Therefore, the ZSVC $V_{0,m}$ is only composed by the third-harmonic component and odd multiplies of the third-harmonic components. In order to testify this point, the test result of the healthy PMSM on experimental platform is analyzed by FFT, as shown in Fig. 3. It is shown that there are only third and ninth (three time of third) harmonic components if higher order harmonics are neglected and this result agrees with the theoretical analysis well.

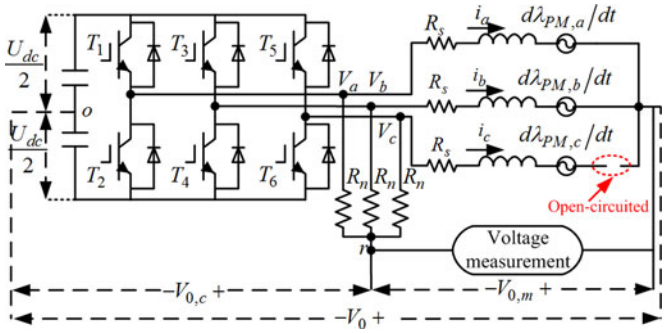

Fig. 4. Configuration of the PMSM with the ISWF in the phase c.

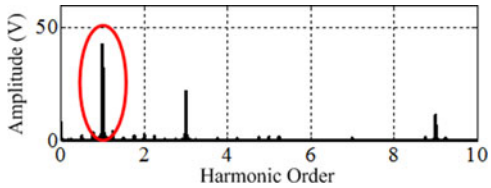

Fig. 5. FFT result of experimental ZSVC $V_{0,m}$ for the ISWF in the phase c, under 30% rated load at 720 r/min.

B. Open-Phase Fault Condition

1) Internal Stator winding failure: Supposing the stator winding of the phase c is open-circuited, as shown in Fig. 4, the voltage equation of the stator phase c does not exist. Hence, the voltage equations of the PMSM with ISWF are expressed as

$$\begin{cases} V_a = R_s i_a + L\dfrac{di_a}{dt} + M\dfrac{di_b}{dt} + \dfrac{d\lambda_{\mathrm{PM},a}}{dt} + V_0 \\ V_b = R_s i_b + M\dfrac{di_a}{dt} + L\dfrac{di_b}{dt} + \dfrac{d\lambda_{\mathrm{PM},b}}{dt} + V_0. \end{cases} \quad (10)$$

In this case, the following conditions are satisfied:

$$\begin{cases} i_a + i_b = 0 \\ i_c = 0. \end{cases} \quad (11)$$

The V_0 can be obtained by adding the rows of (10). Considering (2) and (11), it is expressed as

$$V_0 = \frac{1}{2}(V_a + V_b) - \frac{1}{2}\frac{d(\lambda_{\mathrm{PM},a} + \lambda_{\mathrm{PM},b})}{dt}. \quad (12)$$

In the case of ISWF, (7) and (8) are still satisfied. By substituting (7) and (12) into (8), it generates

$$V_{0,m} = \frac{1}{6}(V_a + V_b) - \frac{1}{3}V_c - \frac{1}{2}\frac{d(\lambda_{\mathrm{PM},a} + \lambda_{\mathrm{PM},b})}{dt}. \quad (13)$$

It is shown from (13) that besides the third harmonic component and its odd multiplies harmonic components, other harmonic components appear in the ZSVC $V_{0,m}$ due to the asymmetry of the PMSM. The FFT result of the experiment $V_{0,m}$ is given in Fig. 5, and it is seen that the amplitude of the fundamental component is largest among those of the new added harmonic components.

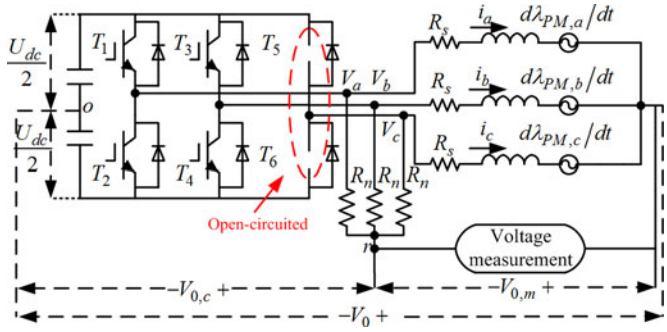

Fig. 6. Configuration of the inverter with TSF in T_5 and T_6.

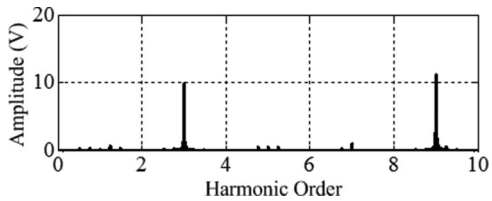

Fig. 7. FFT result of experimental ZSVC $V_{0,m}$ for the TSF in T_5 and T_6, under 30% rated load at 720 r/min.

2) TSF of the Same Leg: The open-circuit fault of switches in the inverter is the common fault and may be classified into individual and multiple failures [24]. If the failure occurs in one switch or two switches in different legs of the inverter, the phase current of the PMSM will not be zero. In this case, the open-circuit fault is easily diagnosed by judging the phase current [24]–[27]. However, the failure of two switches of the same leg will lead to the same phenomenon as the ISWF where the faulty phase has no current and is difficult to discriminate them out.

In this paper, two switches T_5 and T_6 with open-circuit failure are supposed, as shown in Fig. 6. Then, the voltage equations of the PMSM can be expressed as

$$\begin{cases} V_a = R_s i_a + L\dfrac{di_a}{dt} + M\dfrac{di_b}{dt} + \dfrac{d\lambda_{\mathrm{PM},a}}{dt} + V_0 \\ V_b = R_s i_b + M\dfrac{di_a}{dt} + L\dfrac{di_b}{dt} + \dfrac{d\lambda_{\mathrm{PM},b}}{dt} + V_0 \\ V_c = \dfrac{d\lambda_{\mathrm{PM},c}}{dt} + V_0. \end{cases} \tag{14}$$

Under the TSF condition, (7), (8), and (11) are all satisfied. By adding the rows of (14) and considering (2) and (11), the V_0 can be obtained as

$$V_0 = \frac{1}{3}(V_a + V_b + V_c) - \frac{d\lambda_{\mathrm{PM},0}}{dt}. \tag{15}$$

By substituting (7) and (15) into (8), it has

$$V_{0,m} = -\frac{d\lambda_{\mathrm{PM},0}}{dt}. \tag{16}$$

It can be seen that the expression of (16) is the same as that of (9), showing that the ZSVC $V_{0,m}$ is not influenced by the failure of the inverter. Fig. 7 shows the FFT result of the experimental waveform $V_{0,m}$ and it is similar to Fig. 3.

TABLE I
SUMMARY OF FLAG AND Flag_{mn} UNDER HEALTHY AND OPEN-PHASE FAULT CONDITIONS

State	Flag	Flag_{mn}		
		Flag_{ab}	Flag_{bc}	Flag_{ca}
Healthy	0	0	0	0
ISWF in Phase *a*	1	0	1	0
ISWF in Phase *b*	1	0	0	1
ISWF in Phase *c*	1	1	0	0
TSF in T_1 and T_2	0	0	1	0
TSF in T_3 and T_4	0	0	0	1
TSF in T_5 and T_6	0	1	0	0

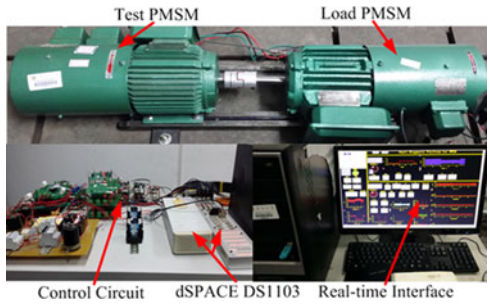

Fig. 8. Experimental Platform.

TABLE II
PARAMETERS OF PMSM

Parameters	Values	Parameters	Values
Number of pole pairs	2	Rated Power (W)	550
Stator resistance (Ω)	10.5	Rated Current (A)	1.5
Flux linkage (Wb)	0.636	Rated Torque (N.·m)	3.5
d-axis inductance (H)	0.16	*q*-axis inductance (H)	0.16

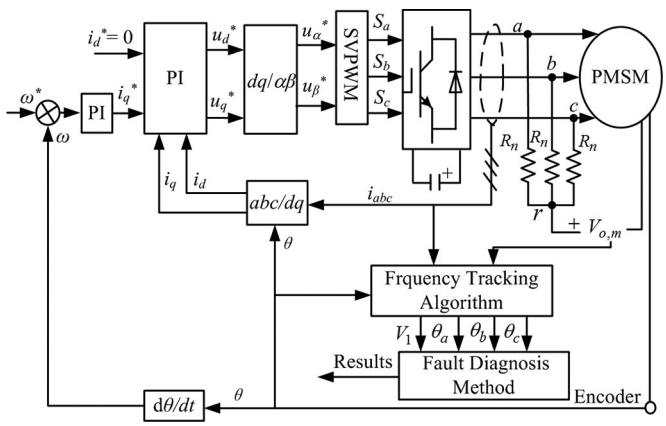

Fig. 9. Control diagram with the proposed fault diagnosis method.

3) Discussion: It can be seen from (9), (13), and (16) that the ISWF is easily detected by the fundamental component of the ZSVC $V_{0,m}$, and ISWF may be discriminated from the TSF and healthy condition. However, the ISWF can be not located in which phase only by ZSVC $V_{0,m}$. It should be noted that

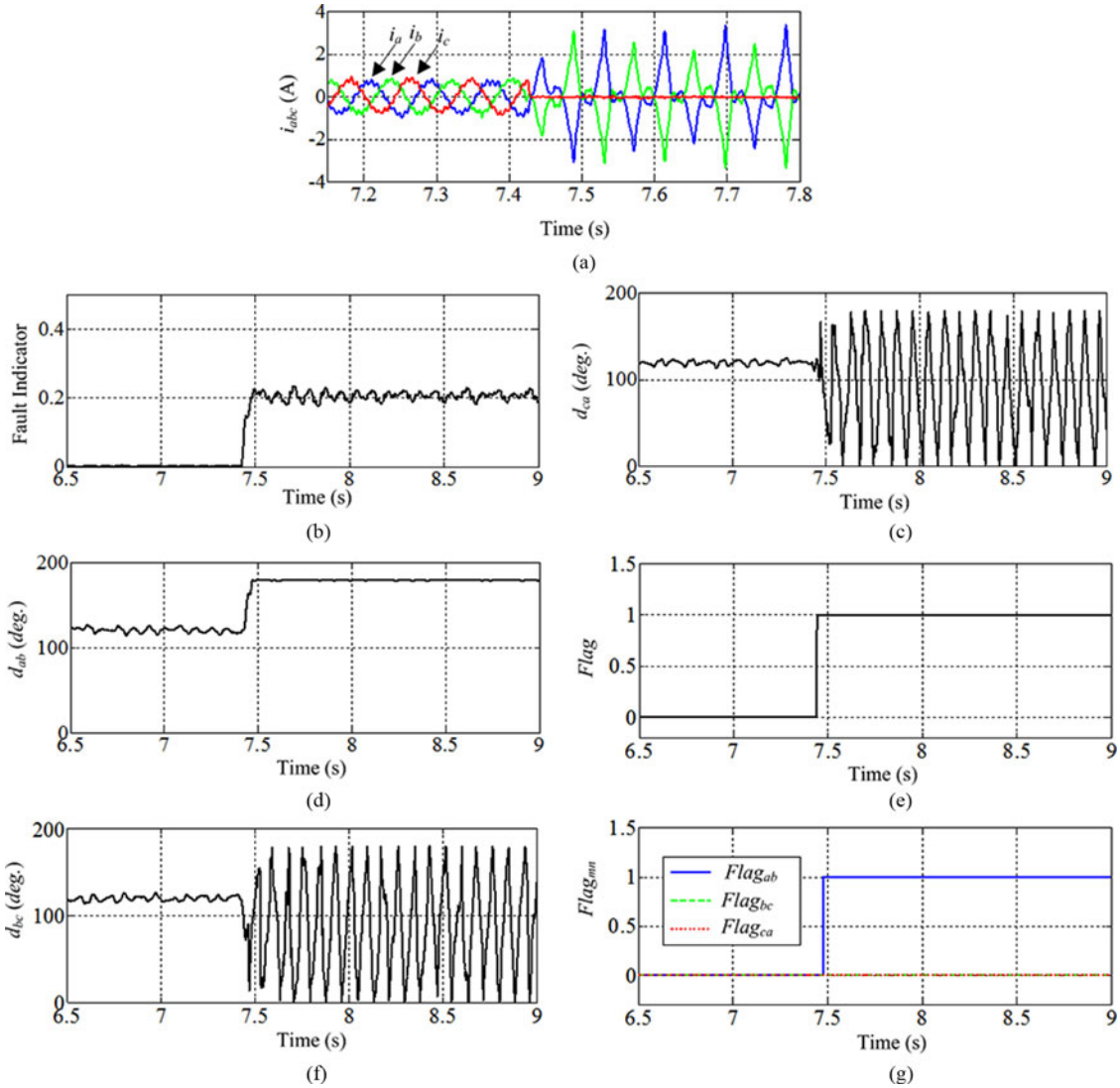

Fig. 10. Experimental results of ISWF, under 30% rated load at 360 r/min. (a) Stator currents. (b) Fault indicator. (c) d_{ab}. (d) d_{bc}. (e) d_{ca}. (f) Flag. (g) Flag_{mn}.

the TSF can be not detected and discriminated from the healthy condition by the fundamental component of the ZSVC $V_{0,m}$.

It is known that the initial phase angle difference of phase-to-phase currents is $2\pi/3$ in a healthy three-phase PMSM, but this does not satisfy under the open--phase fault, where the initial phase angle difference of the currents in the remaining two phases is π. In this case, the initial phase angle differences of the stator currents may be used to analyze the location of the open-phase fault and discriminate the TSF from the healthy condition.

Hence, a combination of the fundamental component of the ZSVC $V_{0,m}$ and the initial phase angle differences of the stator currents are used in this paper to realize the detection, location, and discrimination of the open-phase fault.

One disadvantage is that the proposed method needs an accessible neutral point of the stator windings to measure the ZSVC. However, the neutral point of the stator windings usually leads out and connects to a redundant inverter leg or dc bus midpoint in the case of fault-tolerant PMSM drive system [17]. Hence, the disadvantage may be offset because the open- phase fault can be detect and discriminated; thus, adapting the appropriate fault-tolerant method and making the drive system more reliable.

C. Frequency Tracking Algorithm

In order to realize rapid detection of the amplitude and initial phase angle of the fundamental component, a simple and effective frequency tracking algorithm will be studied. If the high-order harmonics are neglected, the ZSVC $V_{0,m}$ can be expressed as

$$V_{0,m} = V_1 \sin(\theta + \theta_{v1}) + V_3 \sin(3\theta + \theta_{v3}) \tag{17}$$

where V_1 and θ_{v1} are the amplitude and initial phase angle of the fundamental component, respectively, and V_3 and θ_{v3} are the amplitude and initial phase angle of the third-harmonic component, respectively.

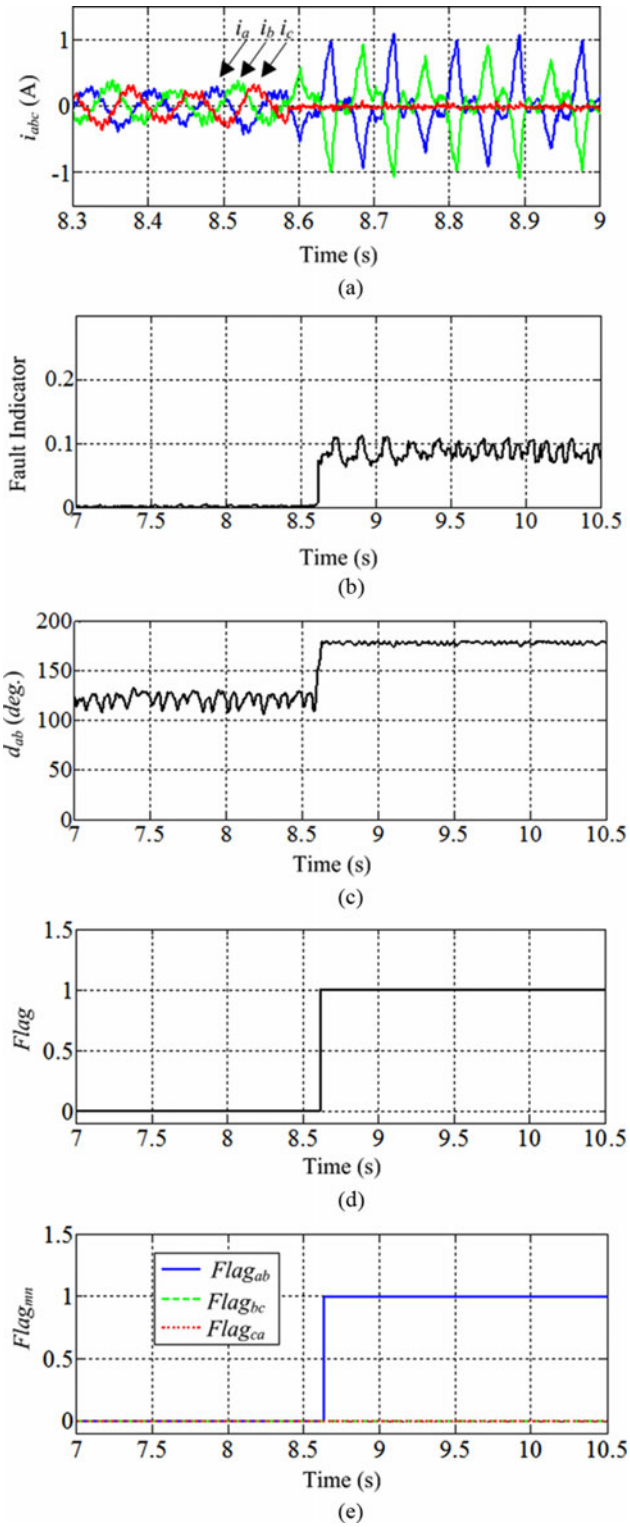

Fig. 11. Experimental results of ISWF, under 10% rated load at 360 r/min. (a) Stator currents. (b) Fault indicator. (c) d_{ab}. (d) Flag. (e) Flagm_{mn}.

Transforming (17) into orthogonal rotating reference frame, the voltage components at d-axis and q-axis are expressed as

$$\begin{cases} V_d = (V_1\sin(\theta+\theta_{v1}) + V_3\sin(3\theta+\theta_{v3}))\cos(\theta) \\ V_q = (V_1\sin(\theta+\theta_{v1}) + V_3\sin(3\theta+\theta_{v3}))\sin(\theta). \end{cases} \tag{18}$$

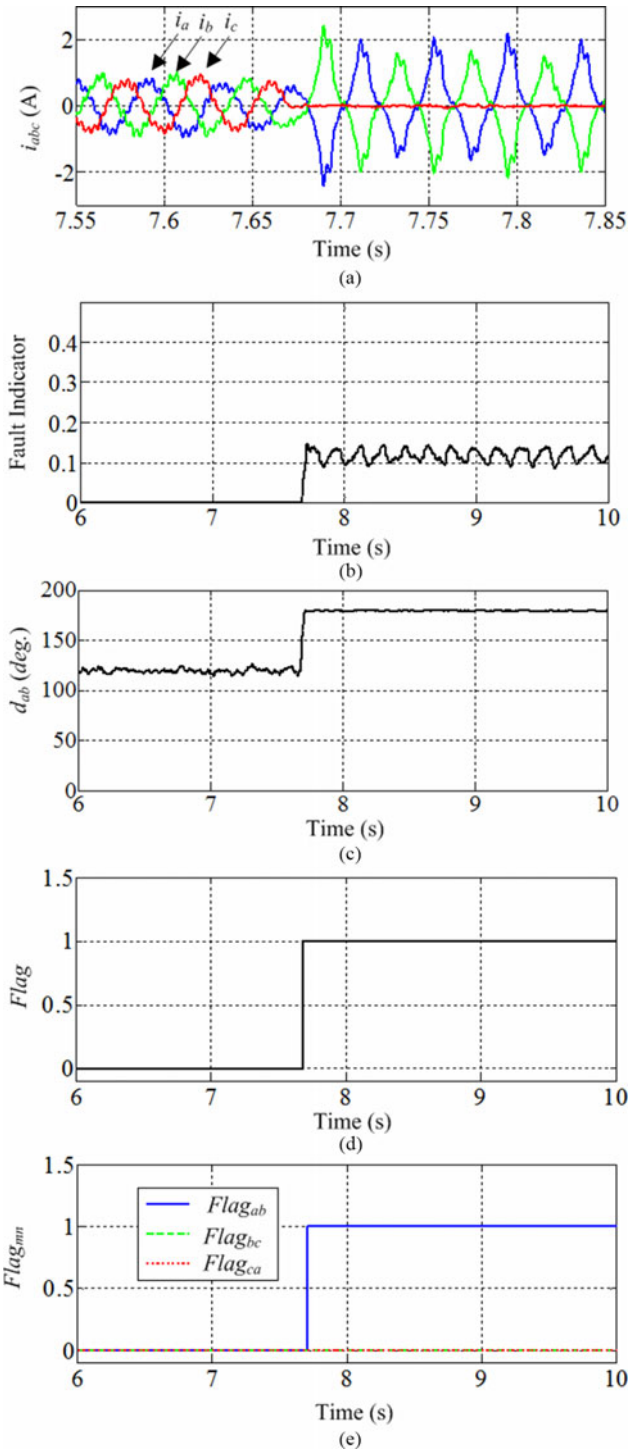

Fig. 12. Experimental results of ISWF, under 30% rated load at 720 r/min. (a) Stator currents. (b) Fault indicator. (c) d_{ab}. (d) Flag. (e) Flag_{mn}.

Using trigonometry identical transformation for (18), it has

$$\begin{cases} V_d = V_1[\sin(2\theta+\theta_{v1}) + \sin(\theta_{v1})]/2 \\ +V_3[\sin(4\theta+\theta_{v3}) + \sin(2\theta+\theta_{v3})]/2 \\ V_q = -V_1[\cos(2\theta+\theta_{v1}) - \cos(\theta_{v1})]/2 \\ -V_3[\cos(4\theta+\theta_{v3}) - \cos(2\theta+\theta_{v3})]/2. \end{cases} \tag{19}$$

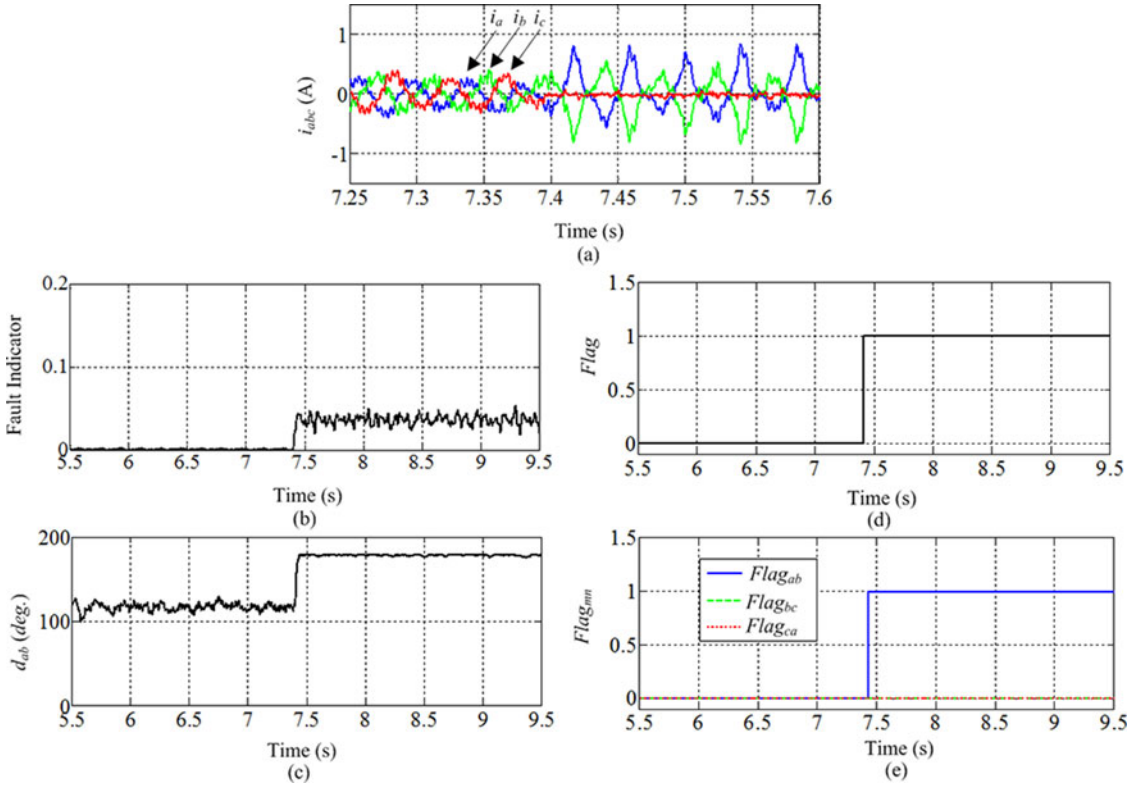

Fig. 13. Experimental results of ISWF, under 10% rated load at 720 r/min. (a) Stator currents. (b) Fault indicator. (c) d_{ab}. (d) Flag. (e) Flag_{mn}.

Filtering the harmonic components of voltage signals from (19), it is

$$\begin{cases} V_{dl} = V_1 \sin(\theta_{v1})/2 \\ V_{ql} = V_1 \cos(\theta_{v1})/2 \end{cases} \tag{20}$$

where V_{dl} and V_{ql} are the dc components of V_d and V_q, respectively. It can be seen from (20) that V_{dl} and V_{ql} are determined by the amplitude and initial phase angle of the fundamental component of the ZSVC $V_{0,m}$. The amplitude and initial phase angle can be calculated as

$$\begin{cases} V_1 = 2\sqrt{V_{dl}^2 + V_{ql}^2} \\ \theta_{v1} = \tan^{-1}(V_{dl}/V_{ql}). \end{cases} \tag{21}$$

It can be seen from (21) that the amplitude and initial phase angle of the ZSVC $V_{0,m}$ can be extracted. Similarly, the amplitude and initial phase angle of the stator currents can be also calculated by the same algorithm.

D. Fault Detection and Discrimination

To achieve fault detection, the amplitude of the ZSVC $V_{0,m}$ is normalized by the dc-link voltage, and the fault indicator is defined as

$$\mathrm{FI} = V_1/U_{\mathrm{dc}} \tag{22}$$

where FI is the fault indicator, V_1 is amplitude of the fundamental component of the ZSVC $V_{0,m}$, and U_{dc} is the dc-link voltage. According to the previous analysis, the fault indicator FI is nearly zero under healthy and TSF conditions where the fundamental component of the ZSVC $V_{0,m}$ does not exist. By defining a threshold for FI value, ISWF can be diagnosed from healthy PMSM and TSF.

The initial phase angle difference d_{mn} is defined as

$$d_{mn} = \begin{cases} |\theta_m - \theta_n| & |\theta_m - \theta_n| <= \pi \\ 2\pi - |\theta_m - \theta_n| & |\theta_m - \theta_n| > \pi \end{cases} \quad m \neq n \in \{a, b, c\} \tag{23}$$

where θ_m and θ_n are the initial phase angles of the fundamental components of the stator currents i_m and i_n, respectively. Therefore, d_{mn} is always $2\pi/3$ as the PMSM is healthy. For example, suppose the open-phase fault occurs in phase c or T_5 and T_6, d_{ab} (where $m = a$, $n = b$) is changed into π, while d_{bc} and d_{ca} are not constant. Therefore, the fault can be detected and the open phase can be located according to the value of d_{mn}.

In order to improve the robustness of the fault diagnosis method, the load torque change and variable speed are taken into consideration since they also lead to the variation of the fault indicator and angle differences. Under healthy condition, when the load torque or the reference speed changes, the fault indicator does not remain zero and angle differences do not remain $2\pi/3$ for a short time during which the controller adjusts the drive to make the PMSM work stably. However, under fault condition, the fault indicator or/and angle differences do not remain the same values as those at healthy state; thus, showing the variation of the fault indicator and angle differences. Thus, it may be not easy to determine whether the variations are caused

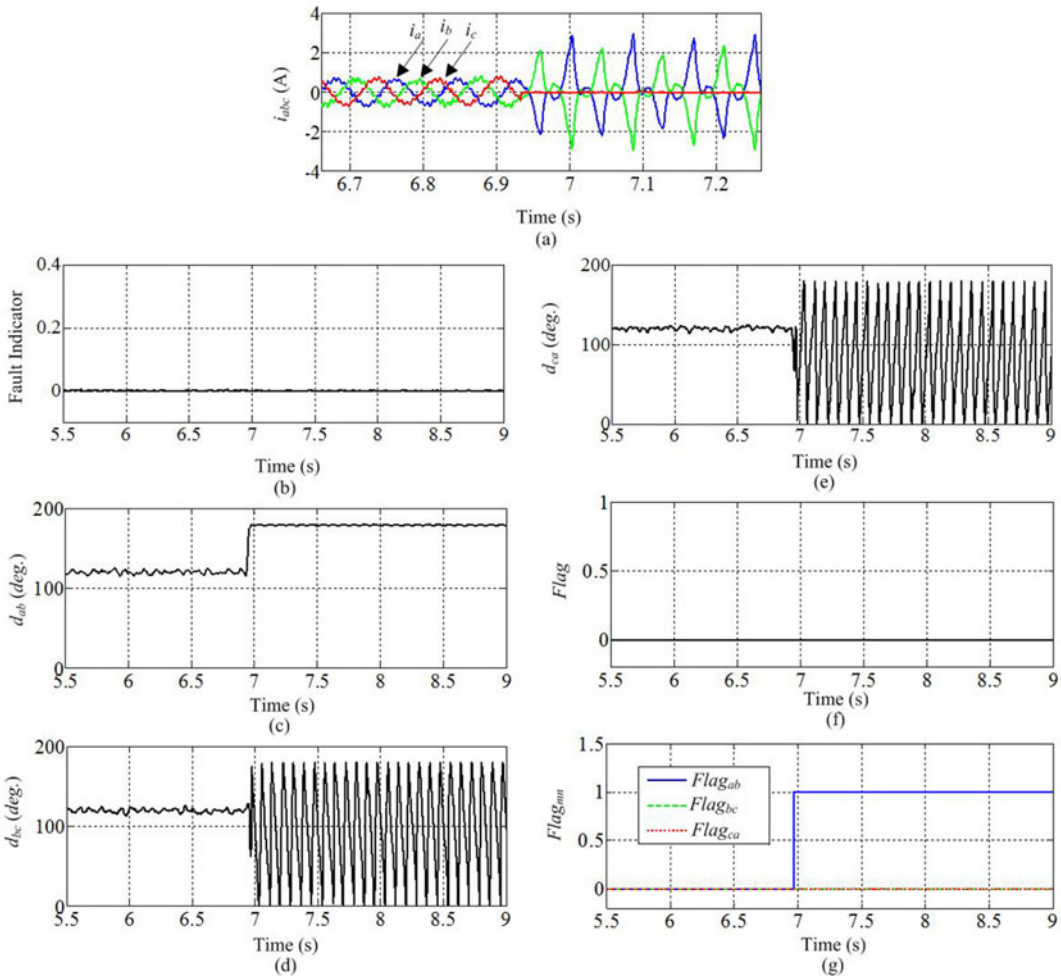

Fig. 14. Experimental results of TSF, under 30% rated load at 360 r/min. (a) Stator currents. (b) Fault indicator. (c) d_{ab}. (d) d_{bc}. (e) d_{ca}. (f) Flag. (g) Flag_{mn}.

by the change of the load and reference speed or open-phase fault. Therefore, the threshold values are employed to deal with this issue and given by

$$\varepsilon = \begin{cases} 1, & \mathrm{FI} >= k_f \\ 0, & \mathrm{FI} < k_f \end{cases} \tag{24}$$

$$\varepsilon_{mn} = \begin{cases} 1, & d_{mn} >= k_d \\ 0, & d_{mn} < k_d \end{cases} \tag{25}$$

where k_f and k_d are the selected threshold values, ε and ε_{mn} are the generated Boolean variables for the fault indicator and angle differences. The threshold values k_f and k_d are positive values and carefully selected to minimize the possibility of the false detection mainly caused by the noises of the measurement and load torque or speed change. If they are not reasonably selected, the probability of the false detection increases.

The detection in (24) and (25) is a simple and frequently used method, but has the possibility of false detection due to the noises of the measurement and load torque or speed change. To guarantee the robustness against the false detection, the same counting algorithm as [27] is applied. The algorithm detects a transition and then starts incrementing a counter till the counter reaches a jitter-free count. If the state is not stable, the counter resets to its initial value. The constant COUNT is defined as how long the Boolean variables are continuously generated and given by

$$\mathrm{COUNT} = k * T/T_s \tag{26}$$

where k is the sensitivity factor, T denotes the current cycle of the PMSM, and T_s stands for the sampling cycle. If k is too large, the open-phase fault may not be detected and discriminated. If k is too small, the possibility of false detection increases. Hence, the sensitivity factor k is carefully selected considering the detection time and reliability of fault detection.

Then, the algorithm for the fault detection and discrimination is given by

$$\mathrm{Flag} = \begin{cases} 1, & \mathrm{counter1} \geq \mathrm{COUNT1} \\ 0, & \mathrm{otherwise} \end{cases} \tag{27}$$

$$\mathrm{Flag}_{mn} = \begin{cases} 1, & \mathrm{counter2} \geq \mathrm{COUNT2} \\ 0, & \mathrm{otherwise} \end{cases} \tag{28}$$

where Flag and Flag_{mn} are the fault detection and discrimination flags, counter1 is the counter value from the beginning of

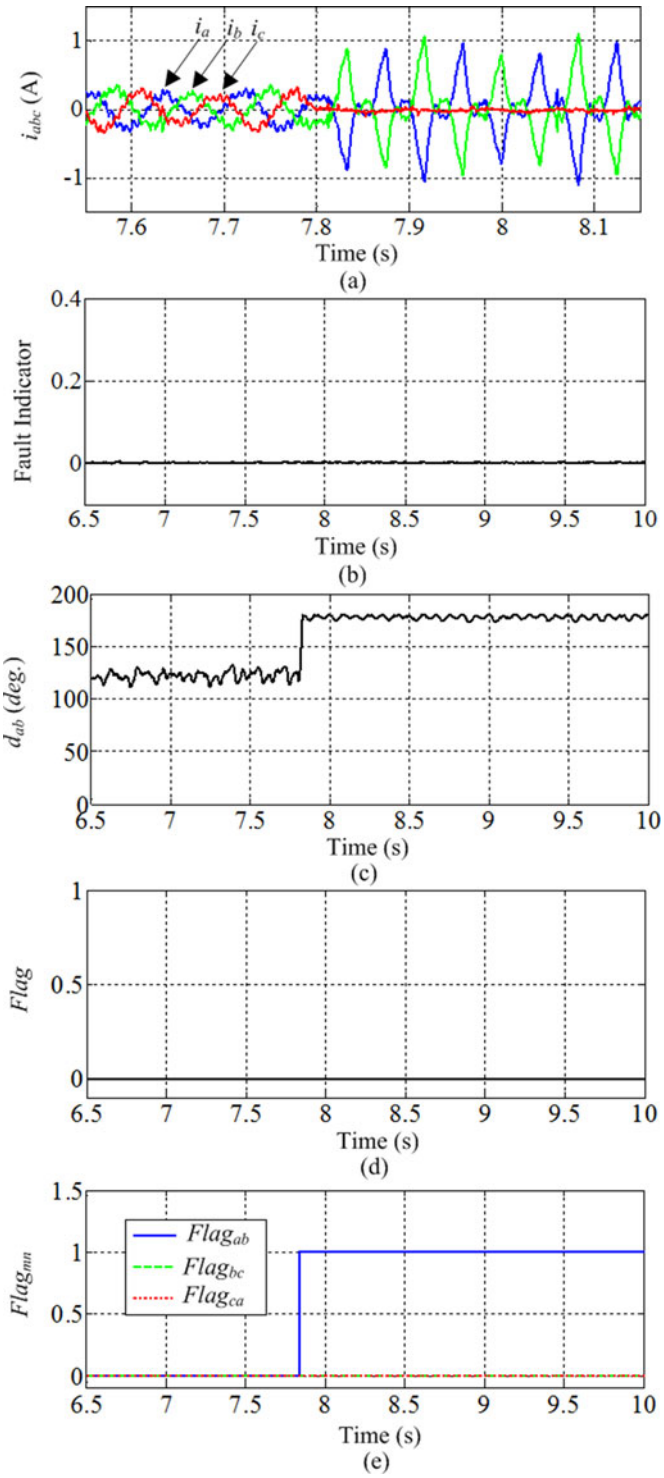

Fig. 15. Experimental results of TSF, under 10% rated load at 360 r/min. (a) Stator current. (b) Fault indicator. (c) d_{ab}. (d) Flag. (e) Flag_{mn}.

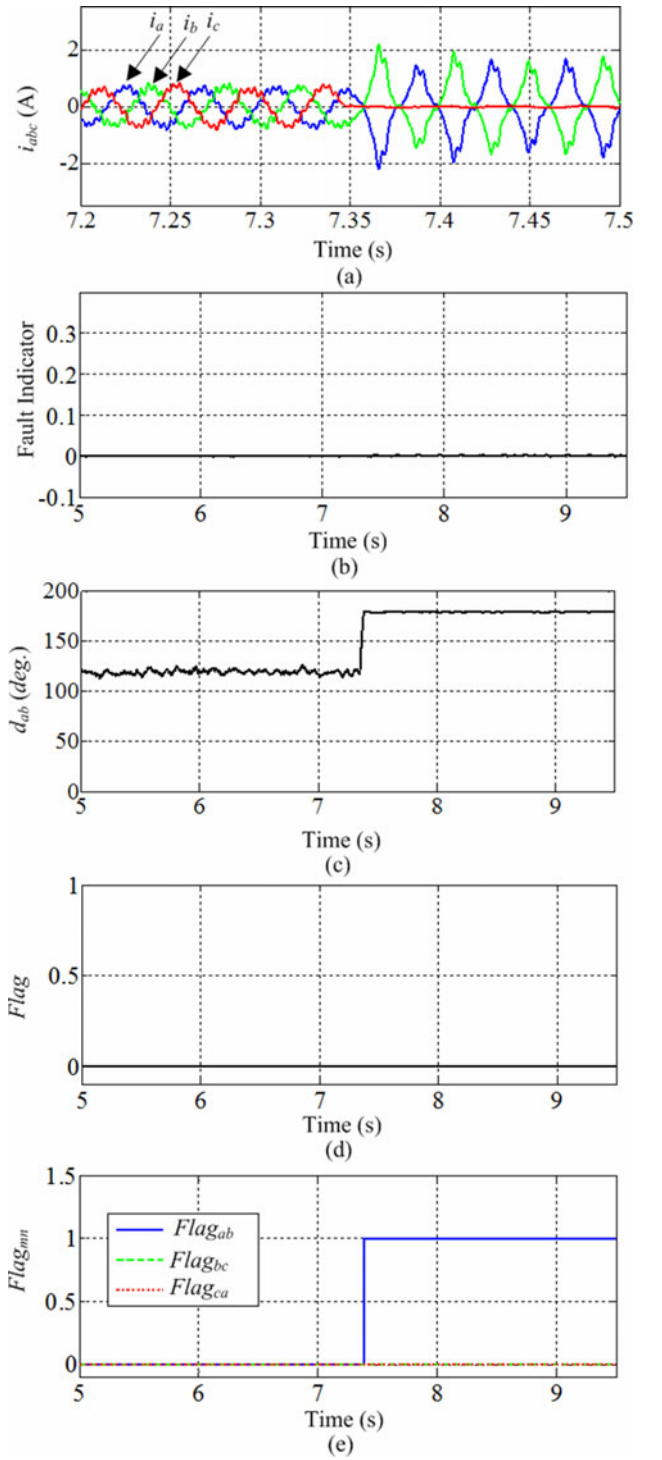

Fig. 16. Experimental results of TSF, under 30% rated load at 720 r/min. (a) Stator currents. (b) Fault indicator. (c) d_{ab}. (d) Flag. (e) Flag_{mn}.

the detection of the Boolean variable $\varepsilon = 1$ in (24) to the arriving at the constant $\mathrm{COUNT1}(\mathrm{COUNT1} = k_1 * T/T_s)$. The counter value counter1 is reset to zero when the Boolean variable is zero. If the counter value counter1 is larger than the constant COUNT1, the Flag is set from low to high. In addition, the counter2, $\mathrm{COUNT2}(\mathrm{COUNT2} = k_2 * T/T_s)$ and Flag_{mn} have the similar definitions to the counter1, COUNT1, and Flag.

Table I presents the summary of the Flag and Flag_{mn} under healthy and open-phase fault conditions. Hence, the open-phase fault can be detected and discriminated by combining the Flag and Flag_{mn}.

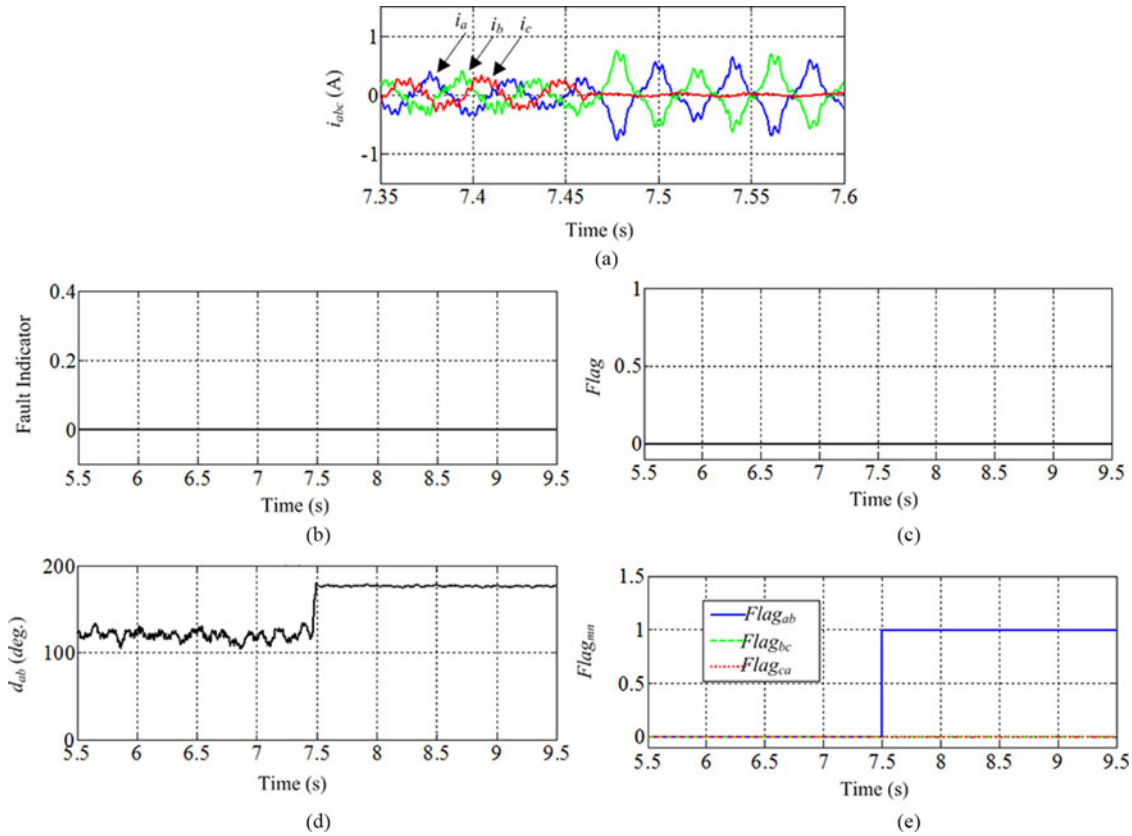

Fig. 17. Experimental results of TSF, under 10% rated load at 720 r/min. (a) Stator currents. (b) Fault indicator. (c) d_{ab}. (d) Flag. (e) Flag_{mn}.

III. Experimental Validation

A. Experimental Platform

To validate the proposed approach, the experimental platform is established, as shown in Fig. 8. Two PMSMs with the same parameters in Table II are coupled together. One of them is used as load of the PMSM. The speed information is obtained by an encoder of 1024 pulses per revolution mounted on the rotor shaft end of the PMSM. The ZSVC $V_{0,m}$ and stator currents are measured directly by voltage sensor and current sensors, respectively. An IGBT-inverter with double closed-loop control system is applied to the test PMSM, as shown in Fig. 9. All the experimental results are carried out at a reference dc-link voltage of 400 V. The value of the resistance in the resistance network is 30 kΩ. The sample frequency of the voltage and current signals is 20 kHz. The parameters (k_f, k_d, k_1, and k_2) of the proposed method are chosen to be 0.005, 170, 0.15, and 0.15 in the tests, respectively. Together with the MATLAB/Simulink and dSPACE ControlDesk, the DS1103 controller provides real-time control and monitoring of the PMSM drive system. In addition, the main frequency of CPU of DS1103 is 933 MHz and computational step size is 5×10^{-5} s.

To evaluate the diagnostic effectiveness, four different operation statuses, namely 30% rated load at a reference speed 360 r/min, 10% rated load at a reference speed 360 r/min, 30% rated load at a reference speed 720 r/min, and 10% rated load at a reference speed 720 r/min are studied.

B. Experimental Results

1) Internal Stator Winding Failure: Fig. 10 shows the experimental results of the stator currents, fault indicator, three initial phase angle differences, and fault detection and discrimination flags, under 30% rated load at 360 r/min, where the ISWF occurs in the phase c at $t = 7.43$ s. It can be seen that under healthy condition the phase currents of the PMSM are balanced, the fault indicator is close to 0, and three angle differences all equal to $2\pi/3$. After the ISWF occurs, the stator current i_c becomes zero and the amplitude of the other two stator currents increases. The fault indicator increases and converges to a value of 0.2. The initial phase angle difference d_{ab} is quickly varied from $2\pi/3$ to π and the others (d_{bc}, d_{ca}) fluctuate in the range of 0 to π. The fault detection and discrimination flags (Flag, Flag_{ab}, Flag_{bc}, Flag_{ca}) are all equal to zero at healthy state. After the ISWF occurrence, the Flag and $\mathrm{Flag}_{\mathrm{ab}}$ are both changed and equal to 1 at the instant $t = 7.47$ s, and Flag_{bc} and Flag_{ca} are not varied, which is agreement with the theoretical analysis. Therefore, the experimental results show that, by combination of the Flag and Flag_{mn}, the ISWF can be effectively detected and located 0.04 s after the fault occurrence, which approximately corresponds to 48% of the PMSM phase current fundamental period.

In order to test the effectiveness of the proposed method, another three experiments with ISWF in phase c are carried out under different operation statuses. The experimental results are shown in Figs. 11–13. It is shown that the fault indicator is nearly equal to zero and initial phase angle difference is hardly

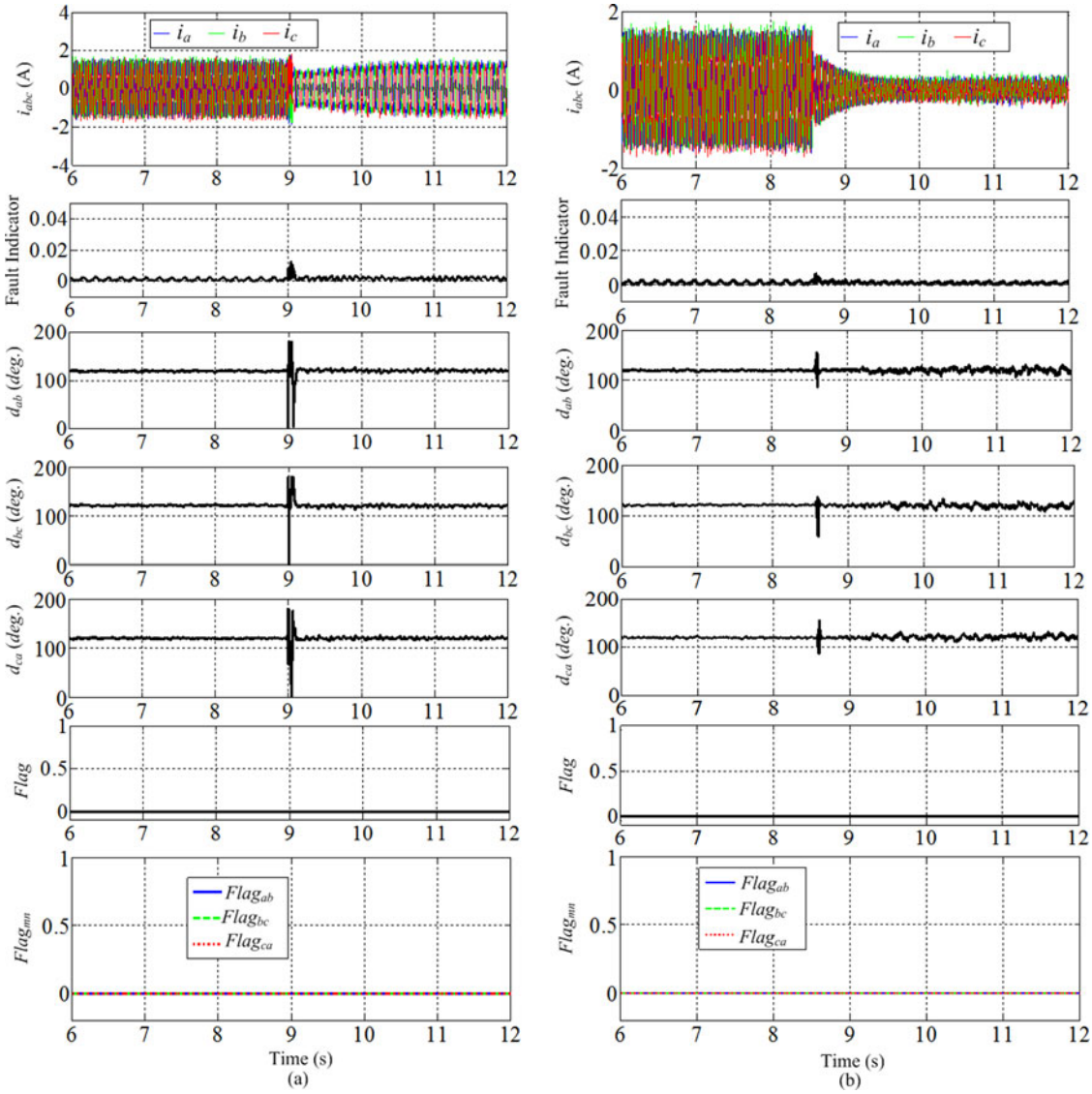

Fig. 18. Experimental results during transient condition. (a) Speed transient. (b) Load transient.

affected by the operation status at normal condition. When the ISWF happens in the phase c, the initial phase angle difference d_{ab} rises to π in all the cases and the fault indicator is affected by operation status. However, the flags (Flag and Flag_{mn}) do not show the false alarms. Hence, the proposed method is still enough to detect the ISWF and locate the faulty phase by the Flag and Flag_{mn}.

2) TSF of the Same Leg: Fig. 14 shows the experimental results of stator currents, fault indicator, three initial phase angle differences, and fault detection and discrimination flags, under 30% rated load at 360 r/min, where the TSF occurs due to T_5 and T_6 at $t = 6.94$ s. It is shown in Fig. 14(a) that the stator currents are similar to the ones in Fig. 10(a). Therefore, the currents-based open-phase fault detection methods introduced in [6]–[9] are invalid to discriminate the fault type since the waveforms of the stator current are nearly same under different fault types, such as ISWF and TSF.

It can be seen from Fig. 14(b) that the fault indicator keeps close to 0 before and after the TSF occurs. The initial phase angle difference d_{ab} rapidly rises from $2\pi/3$ to π and the others (d_{bc}, d_{ca}) fluctuate in the range of 0 to π, as shown in Fig. 14(c)–(e). This is similar to the case of ISWF, as shown in Fig. 10(c)–(e). Furthermore, the Flag, Flag_{bc}, and Flag_{ca} are always equal to 0 before and after the TSF occurrence, while at the instant $t = 6.967$ s, the Flag_{ab} is changed into 1, which is agreement with the summary listed in Table I. Hence, the experimental results show that the TSF can be detected and located in a time interval of about 0.037 s by combination of the Flag and Flag_{mn}, which is approximately equivalent to 44% of the PMSM phase current fundamental period.

Similarly, further experiments are done for the TSF in T_5 and T_6 to verify the effectiveness of the proposed method. The experimental results are shown in Figs. 15–17, where the fault indicator and initial phase angle difference are hardly affected by operation status. The experimental results indicate that, under different operations statues, the TSF can be still detected and discriminated from the ISWF and healthy conditions by combination of the Flag and Flag_{mn}.

So far, all the experiments are focused on the ISWF in the phase c or the TSF in T_5 and T_6. The extensive experiments are also performed for the other phases or switches. Similar experiment results are obtained as expected, which proves that the proposed method is capable of detecting the open-phase fault, locating the fault phase or inverter leg, and discriminating the fault types.

3) Transient Behavior: In order to further validate the performance of the proposed method, the experiments for the healthy PMSM under transient conditions are carried out, and the experimental results are presented in Fig. 18. Fig. 18(a) shows the experimental results for the speed transient, at the moment $t = 8.99$ s, from 720 to 360 r/min and by considering 60% rated load. Fig. 18(b) shows the experiment results for the load transient, at the instant $t = 8.56$ s, from 60% rated load to 10% rated load and by considering the PMSM reference speed 720 r/min. It can be seen that the fault indicator and angle differences all have a transient process under two transient conditions. The fault indicator and angle differences are hardly varied before and after the transient process, except the angle differences with a little large ripple under light-load condition. In the two cases, these experimental results also prove that the Flag and Flag_{mn} are still kept zero before and after the speed and load transients. Therefore, it can be confirmed that the chosen threshold values allow the proposed diagnostic method to handle the extreme situations, the speed and load transients, without emitting false alarms.

IV. Conclusion

In this paper, a new detection and discrimination method for the open-phase fault in the PMSM drive system is proposed, which not only can detect the open-phase fault, but also can discriminate the fault types, ISWF and TSF. The ZSVC is first analyzed under healthy and open-phase fault conditions. Then, the frequency tracking algorithm is proposed to extract the amplitude and initial phase angle in time domain, and the fault indicator and initial phase angle differences are calculated in real time. Furthermore, to guarantee the robustness of the proposed method, the threshold values and Counting algorithm are adopted. Finally, the detection and discrimination of the open-phase fault are presented by combination of the flags: Flag and Flag_{mn}. To verify the proposed method, the experiments are carried out, and the results agree with the theoretical analysis well.

It should be noted that an accessible neutral point of the stator windings is needed to measure the ZSVC. However, the neutral point is accessible for fault-tolerant PMSM drive system, where the combination of the proposed fault detection method and fault-tolerant method may improve the reliability of the PMSM drive system greatly.

References

[1] M. Cheng and Y. Zhu, "The state of the art of wind energy conversion systems and technologies: A review," *Energy Convers. Manage.*, vol. 88, pp. 332–347, Dec. 2014.

[2] W. Wang, M. Cheng, B. Zhang, Y. Zhu, and S. Ding, "A fault-tolerant permanent magnet traction module for subway application," *IEEE Trans. Power Electron.*, vol. 29, no. 4, pp. 1646–1658, Apr. 2014.

[3] M. Cheng and C.C. Chan, "General requirement of traction motor drives" in *Encyclopedia of Automotive Engineering*, D. Crolla, D.E. Foster, T. Kobayashi, and N. Vaughan, Eds. Chichester, U.K.: Wiley, Apr. 2014.

[4] S. Nandi, H. A. Toliyat, and X. D. Li, "Condition monitoring and fault diagnosis of electrical motors—A review," *IEEE Trans. Energy Convers.*, vol. 20, no. 4, pp. 719–729, Dec. 2005.

[5] B. A. Welchko, T. M. Janhns, and S. Hiti, "IPM synchronous machine drive response to a single-phase open circuit fault," *IEEE Trans. Power Electron.*, vol. 17, no. 5, pp. 764–771, Sep. 2002.

[6] C. J. Gajanayake, B. Bhangu, S. Nadarajan, and G. Jayasinghe, "Fault tolerant control method to improve the torque and speed response in PMSM drive with winding faults," in *Proc. IEEE Int. Conf. Power Electron. Drive Syst.*, 2011, pp. 956–961.

[7] A. Khlaief, M. Boussak, and M. Gossa, "Open phase faults detection in PMSM drives based on current signature analysis," in *Proc. IEEE Int. Conf. Electr. Mach.*, 2010, pp. 1–6.

[8] A. Kontarcek, P. Bajec, M. Nemec, and V. Ambrozic, "Single open-phase fault detection in permanent magnet synchronous machine through current predication," in *Proc. IEEE Annu. Conf. Ind. Electron. Soc.*, 2013, pp. 5860–5865.

[9] S. S. Kuruppu and A. Kulatunga, "D-Q current signature based faulted phase localization for SM-PMAC machine drive," *IEEE Trans. Ind. Electron.*, vol. 2, no. 1, pp. 113–121, Jan. 2015.

[10] R. Ribeiro, C. Jacobina, E. da Silva, and A. Lima, "Fault detection of open-switch damage in voltage-fed PWM motor drive systems," *IEEE Trans. Power Electron.*, vol. 18, no. 2, pp. 587–593, Mar. 2003.

[11] Q. T. An, L. Z. Sun, K. Zhao, and L. Sun, "Switching function model based fast-diagnostic method of open-switch faults in inverters without sensors," *IEEE Trans. Power Electron.*, vol. 26, no. 1, pp. 119–126, Jan. 2011.

[12] M. A. Rodriguez-Blanco, A. Claudio-Sanchez, D. Theilliol, L. G. Vela-Valdes, P. Sibaja-Teran, L. Hernandez-Gonzalez, and J. Aguayo-Alquicira, "A failure-detection strategy for IGBT based on gate-voltage behavior applied to a motor drive system," *IEEE Trans. Ind. Electron.*, vol. 58, no. 5, pp. 1625–1633, May 2011.

[13] C. Choi and W. Lee, "Design and evaluation of voltage measurement based sectoral diagnosis method for inverter open switch faults of permanent magnet synchronous motor drives," *IET Electr. Power App.*, vol. 6, no. 8, pp. 526–532, Sep. 2012.

[14] S. M. Jung, J. S. Park, and H. W. Kim, "An MRAS-based diagnosis of open-circuit fault in PWM voltage-source inverters for PM synchronous motor drive systems," *IEEE Trans. Power Electron.*, vol. 28, no. 5, pp. 2514–2526, May 2013.

[15] N. M. A. Freier, J. O. Estima, and A. J. M. Cardoso, "A voltage-based approach without extra hardware for open-circuit fault diagnosis in closed-loop PWM AC regenerative drives," *IEEE Trans. Ind. Electron.*, vol. 61, no. 9, pp. 4960–4970, Sep. 2014.

[16] B. A. Welchko, T. A. Lipo, T. M. Jahn, and S. E. Schulz, "Fault tolerant three-phase AC motor drive topologies: A comparison of features, cost, and limitations," *IEEE Trans. Power Electron.*, vol. 19 no. 4, pp. 1108–1116, Jul. 2004.

[17] D. U. Campos-Delgado, D. R. Espinoza-Trejo, and E. Palacios, "Fault-tolerant control in variable speed drives: A survey," *IET Elect. Power Appl.*, vol. 2, no. 2, pp. 121–134, Mar. 2008.

[18] R. R. Errabelli and P. Mutschler, "Fault-tolerant voltage source inverter for permanent magnet drives," *IEEE Trans. Power Electron.*, vol. 27, no. 2, pp. 500–508, Feb. 2012.

[19] T. H. Liu, J. R. Fu, and T. A. Lipo, "A strategy for improving reliability of field-oriented controlled induction motor drives," *IEEE Trans. Ind. Appl.*, vol. 29, no. 5, pp. 910–917, Sep./Oct. 1993.

[20] S. Bolognani, M. Zordan, and M. Zigliotto, "Experimental fault-tolerant control of a PMSM drive," *IEEE Trans. Ind. Electron.*, vol. 47, no. 5, pp. 1134–1141, Oct. 2000.

[21] J. C. Urresty, J. R. Riba, and L. Romeral, "Application of the zero-sequence voltage component to detect stator winding inter-turn faults in PMSMs," *Electr. Power Syst. Res.*, vol. 89, pp. 38–44, Aug. 2012.

[22] J. Hang, J. Zhang, M. Cheng, and J. Huang, "Online interturn fault diagnosis of permanent magnet synchronous machine using zero-sequence components," *IEEE Trans. Power Electron.*, vol. 30, no. 12, pp. 6731–6741, Dec. 2015.

[23] J. C. Urresty, J. R. Riba, and L. Romeral, "Diagnosis of interturn faults in PMSMs operating under nonstationary conditions by applying order

tracking filtering," *IEEE Trans. Power Electron.*, vol. 28, no. 1, pp. 507–515, Jan. 2013.
[24] W. Sleszynski, J. Nieznanski, and A. Cichowski, "Open-transistor fault diagnostics in voltage-source inverters by analyzing the load currents," *IEEE Trans. Ind. Electron.*, vol. 56, no. 11, pp. 4681–4688, Nov. 2009.
[25] J. O. Estima and A. J. M. Cardoso, "A new approach for real-time multiple open-circuit fault diagnosis in voltage source inverters," *IEEE Trans. Ind. Appl.*, vol. 47, no. 6, pp. 2487–2494, Nov./Dec. 2011.
[26] J. O. Estima and A. J. M. Cardoso, "A new algorithm for real-time multiple open-circuit fault diagnosis in voltage-fed PWM motor drives by the reference current errors," *IEEE Trans. Ind. Electron.*, vol. 60, no. 8, pp. 3496–3505, Aug. 2013.
[27] J. Zhang, J. Zhao, D. Zhou, and C. Huang, "High-performance fault diagnosis in PWM voltage-source inverters for vector-controlled induction motor drives," *IEEE Trans. Power Electron.*, vol. 29, no. 11, pp. 6087–6099, Nov. 2014.

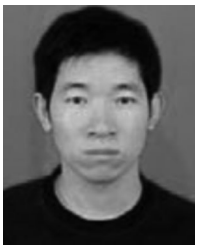

Jun Hang (S'12) received the B.Sc. and M.Sc. degrees in electrical engineering from the Anhui University of Science and Technology, Huainan, China, in 2008 and 2011, respectively. He is currently working toward the Ph. D degree in electrical engineering at Southeast University, Nanjing, China.

His current research interests include condition monitoring, fault diagnosis, and wind power generation.

Jianzhong Zhang (M'08) received the M.Sc. and Ph.D. degrees in electrical engineering from the Department of Electrical Engineering, Southeast University, Nanjing, China, in 2005 and 2008, respectively.

Since 2008, he has been with Southeast University, where he is currently a Research Professor at the School of Electrical Engineering. In recent years, he has authored and coauthored more than 80 technical papers and 25 Chinese patents. His research interests include electric machines, power electronics, and wind power generation.

Ming Cheng (M'01–SM'02–F'15) received the B.Sc. and M.Sc. degrees from the Department of Electrical Engineering, Southeast University, Nanjing, China, in 1982 and 1987, respectively, and the Ph.D. degree from the Department of Electrical and Electronic Engineering, The University of Hong Kong, Hong Kong, in 2001.

Since 1987, he has been with Southeast University, where he is currently a Professor at the School of Electrical Engineering and the Director of the Research Center for Wind Power Generation. His teaching and research interests include electrical machines, motor drives for electric vehicles, and renewable energy generation. He has authored or coauthored more than 300 technical papers and four books and is the holder of 60 patents in these areas.

Prof. Cheng is a Fellow of the Institution of Engineering and Technology. He has served as the Chair and Organizing Committee Member for many international conferences. He is a Distinguished Lecturer of the IEEE Industry Applications Society in 2015/2016.

Shichuan Ding (S'08–S'12) received the B.Sc. degree in electrical engineering from Anhui University, Hefei, China, in 2001, and the M.Sc. degree from USTC, Hefei, China, in 2006. He is currently working toward the Ph.D. degree in electrical engineering at Southeast University, Nanjing, China.

His research interests include electrical machine drive, power electronics applications, and energy management in EVs.